



# Geophysical Research Letters

## RESEARCH LETTER

10.1029/2019GL085580

### Key Points:

- Melting of sea ice in the Navy-ESPC model is locally enhanced by an intense cyclone
- The enhanced melting is short-lived and spatially confined
- Overall sea ice extent does not change in association with the cyclone

### Supporting Information:

- Supporting Information S1

### Correspondence to:

D. P. Stern,  
dstern@ucar.edu

### Citation:

Stern, D., P. Doyle, J. D., Barton, N. P., Finocchio, P. M., Komaromi, W. A., & Metzger, E. J. (2020). The impact of an intense cyclone on short-term sea ice loss in a fully coupled atmosphere-ocean-ice model. *Geophysical Research Letters*, 47, e2019GL085580. <https://doi.org/10.1029/2019GL085580>

Received 26 SEP 2019

Accepted 25 JAN 2020

Accepted article online 29 JAN 2020

## The Impact of an Intense Cyclone on Short-Term Sea Ice Loss in a Fully Coupled Atmosphere-Ocean-Ice Model

Daniel P. Stern<sup>1</sup>, James D. Doyle<sup>2</sup>, Neil P. Barton<sup>2</sup>, Peter M. Finocchio<sup>3</sup>, William A. Komaromi<sup>2</sup>, and E. Joseph Metzger<sup>4</sup>

<sup>1</sup>University Corporation for Atmospheric Research, Monterey, CA, USA, <sup>2</sup>Naval Research Laboratory, Monterey, CA, USA, <sup>3</sup>National Research Council, Monterey, CA, USA, <sup>4</sup>Naval Research Laboratory, Stennis Space Center, MS, USA

**Abstract** Arctic cyclones may be associated with periods of locally enhanced sea ice loss during the summer, and some studies have found that an intense cyclone in August 2012 resulted in a rapid sea ice retreat. This study uses a coupled atmosphere-ocean-ice model (Navy-ESPC) to explore the relationship between the 2012 cyclone and short-term sea ice melting. There are two mechanisms of cyclone-induced melting in Navy-ESPC: turbulent mixing of a warm layer located at 15- to 35-m depth increases bottom melting and warm air advection by the strong surface winds increases surface melting. Although the rate of sea ice melt is substantially increased in association with the cyclone, this effect is confined to a relatively small region and only lasts for a few days. There is no clear signature of the cyclone on the overall Arctic sea ice extent in Navy-ESPC.

**Plain Language Summary** Cyclones (storms) over the Arctic Ocean may be associated with periods of locally enhanced sea ice loss during the summer, and some studies have found that an intense cyclone in August 2012 resulted in a rapid sea ice retreat. This study uses a computer model (Navy-ESPC) that includes interactions between the atmosphere, the ocean, and the sea ice, to explore the relationship between the 2012 cyclone and short-term sea ice melting. In this model, there are two mechanisms by which melting of sea ice is enhanced by the cyclone: (1) warm water from below is mixed upward, which increases the rate of melting on the bottom of the sea ice, and (2) warm air is brought northward by the strong winds of the cyclone, which increases the rate of melting on the top of the sea ice. These two mechanisms combine to substantially increase the rate of melting of sea ice, but the effect of the cyclone on the sea ice is confined to a relatively small region and only lasts for a few days. In this model, there is no clear effect of the cyclone on the overall extent of the sea ice over the Arctic Ocean.

## 1. Introduction

Every summer, the Arctic Ocean loses approximately 70% of its ice extent (Meier & Stewart, 2019), transitioning from nearly complete ice coverage to a state where most of the Arctic is either ice free or is covered by a broad region of dispersed and thin ice. On a seasonal time scale, the reason for this loss of ice is well understood (Perovich et al., 2008): increasing solar insolation following months of darkness melts the ice both from above (from absorption of shortwave radiation) and below (by warming the oceanic mixed layer that is in contact with the overlying ice), and eventually, regions of thin ice are melted away entirely, reducing ice concentration and decreasing ice extent. On shorter time scales (days to weeks), there is large variability in space and time in the rate of melting and consequent decrease in concentration and thickness. A number of different processes have been argued to regulate the rate of ice loss on such time scales, including variations in cloud cover (Kay et al., 2008), anomalous advection of warm and moist air over the ice (Park et al., 2015; Woods & Caballero, 2016), and upward mixing of relatively warm water from beneath the oceanic mixed layer (Jackson et al., 2012; Zhang et al., 2013; Watanabe & Ogi, 2013). Each of these processes may be influenced by the synoptic-scale weather, and the inability to predict such weather beyond 1–2 weeks may be responsible for the limited skill of seasonal sea ice extent forecasts (Serreze et al., 2016; Stroeve et al., 2014).

Several studies have suggested that intense cyclones may be responsible for anomalously large ice loss (Jackson et al., 2012; Simmonds & Rudeva, 2012; Parkinson & Comiso, 2013; Zhang et al., 2013). Zhang et al. (2013) used the Pan-Arctic Ice-Ocean Modeling and Assimilation System (PIOMAS) (Zhang & Rothrock, 2003) to investigate the effect of a particularly intense cyclone in August 2012 (Simmonds & Rudeva, 2012)

on the loss of sea ice. They found that strong surface wind speeds induced a substantial enhancement of turbulent vertical mixing within the ocean, resulting in entrainment of warm water into the mixed layer from below and a notable increase in the rate of bottom melting of sea ice over a large region of the Pacific sector of the Arctic Ocean. However, they also determined through a sensitivity experiment that almost all of the additional ice that melted as a result of the cyclone would have eventually melted anyway later in the summer, and so they concluded that the cyclone did not substantially influence the seasonal minimum extent in 2012, which was a record low. The PIOMAS simulations of Zhang et al. (2013) were forced by NCEP/NCAR daily atmospheric reanalysis fields. As far as we are aware, no study has yet investigated the phenomenon of cyclone-induced sea ice melt in a fully coupled atmosphere-ocean-ice model, and it is the purpose of this study to do so.

## 2. Model Description and Forecast Evaluation

We use the Navy Earth System Prediction Capability (Navy-ESPC) system (Barton et al., 2019), which is a fully coupled global model composed of the Navy Global Environmental Model (NAVGEOM) (Hogan et al., 2014), the HYbrid Coordinate Ocean Model (HYCOM) (Metzger et al., 2014), and the Community Ice Code model (CICE version 4.0, Hunke & Lipscomb, 2010). Further details on the model setup (which is the same as is used in the SubX project Pegion et al., 2019) are given in the supporting information.

We evaluated multiple initializations of the Navy-ESPC forecasts in comparison to the ERA-Interim (ERA-I) Reanalysis (Figure S1). Navy-ESPC forecasts initialized 1–2 days prior to the occurrence of peak intensity (12 UTC 6 August for pressure and 12 UTC 5 August for wind speed) do reasonably well at predicting the evolution of the cyclone (Figures S1a and S1b), but the time window of predictability appears to be rather short (consistent with Yamagami et al., 2018). Because of its relatively skillful prediction of the cyclone, we focus our subsequent analysis on the forecast initialized at 12 UTC 4 August. In the 36-hr forecast valid at 00 UTC 6 August (and in ERA-I), the strongest wind speeds are found in an elongated band originating just north of the cyclone center, wrapping around to the east, and extending to the south over far northwestern Alaska (Figures S1c and S1d). This maximum wind speed band is within the warm sector of the cyclone (where 15- to 20-m  $s^{-1}$  winds are widespread), and the western edge of the band is coincident with the surface cold front (Figure 1b). Given the good correspondence between the short-term forecast of the cyclone and the ERA-I Reanalysis, it is reasonable to further examine this simulation in order to investigate the relationship between the cyclone and sea ice melt in the coupled Navy-ESPC model.

## 3. Mechanisms of Cyclone-Induced Sea Ice Melt in Navy-ESPC

Figures 1a and 2a show the instantaneous rate of surface melting and bottom (plus lateral) melting for the 36-hr Navy-ESPC forecast, respectively. Surface melting is small over most of the Arctic at this time, as solar insolation declines sharply in August (Flocco et al., 2012; Steele et al., 2010), and surface air temperatures over the ice at this time are typically at or below  $0^{\circ}C$  (Lüpkes et al., 2010; Persson et al., 2002). There is a wedge-shaped region of rapid surface melting that is coincident with the warm sector of the cyclone, which can be seen in the 2-m air temperature (Figure 1b). The strong surface winds advect much warmer air poleward from the continents and areas of open water, and this warm air enhances surface melting of the ice through increased sensible heat fluxes (Figure 1c). Figure 1d shows the shortwave radiation that is absorbed by the ice, and it can be seen that there is also a region of locally large radiative forcing (associated with reduced cloud cover in the warm sector relative to the frontal regions, not shown) that is approximately coincident with the area of enhanced surface melting. However, the strength of this radiative forcing within the warm sector is actually similar to that at times prior to and after the passage of the cyclone, whereas the sensible heating is greatly enhanced during the passage of the cyclone. Figure 1e shows the surface energy budget averaged over the ice-covered region from  $70^{\circ}$ – $80^{\circ}N$  and  $130^{\circ}$ – $170^{\circ}W$ , from 00 UTC 5 August to 00 UTC 12 August. The absorbed shortwave radiation decreases from  $199$  to  $187$   $W m^{-2}$ , while the sensible heat flux increases from  $1$  to  $45$   $W m^{-2}$  (positive values indicate a net flux into the ice), between 00 UTC on 5 and 6 August. Finally, Figure 1f compares the net energy flux into the ice to the area-averaged rate of surface melting, and the good correspondence between these two time series and that of the sensible heat flux (Figure 1e) indicates that the primary mechanism of enhanced surface melting in association with the cyclone is the increased sensible heating from warm air advection, rather than changes in the radiative forcing.

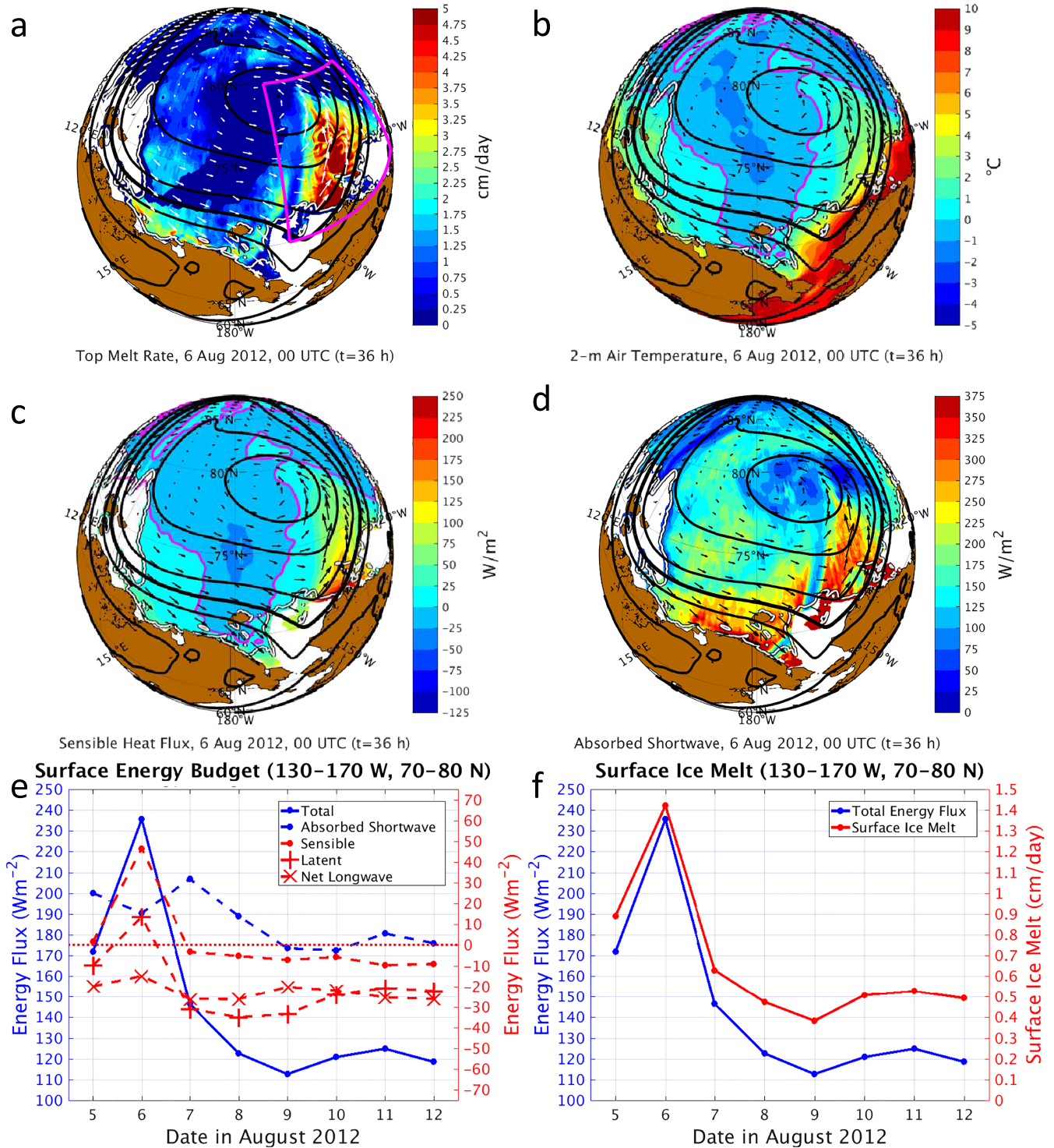


**Figure 1.** For the Navy-ESPC forecast initialized at 12 UTC 4 August 2012, 36-hr forecasts of (a) surface melt rate, (b) 2-m air temperature, (c) sensible heat flux from the atmosphere to the ice, and (d) shortwave radiation absorbed by the ice (including absorption by the ocean at grid points with ice concentration less than 100%). In (a)–(d), sea level pressure is contoured in black every 8 mb (with the 1,000-mb contour thickened), the 15% ice concentration contour is in white, and the vectors indicate the ice velocity. The magenta contour in (b) and (c) indicates the 0°C air temperature. Note that the color bars of (c) and (d) differ. Fluxes are defined such that positive values are into the ice. (e) The ice surface energy budget and (f) the instantaneous rate of surface melting, averaged over 130–170°W and 70–80°N (indicated by the magenta box in (a)). Note that rate of melting in (a) is per unit grid cell area, whereas that in (f) is per unit area of ice.

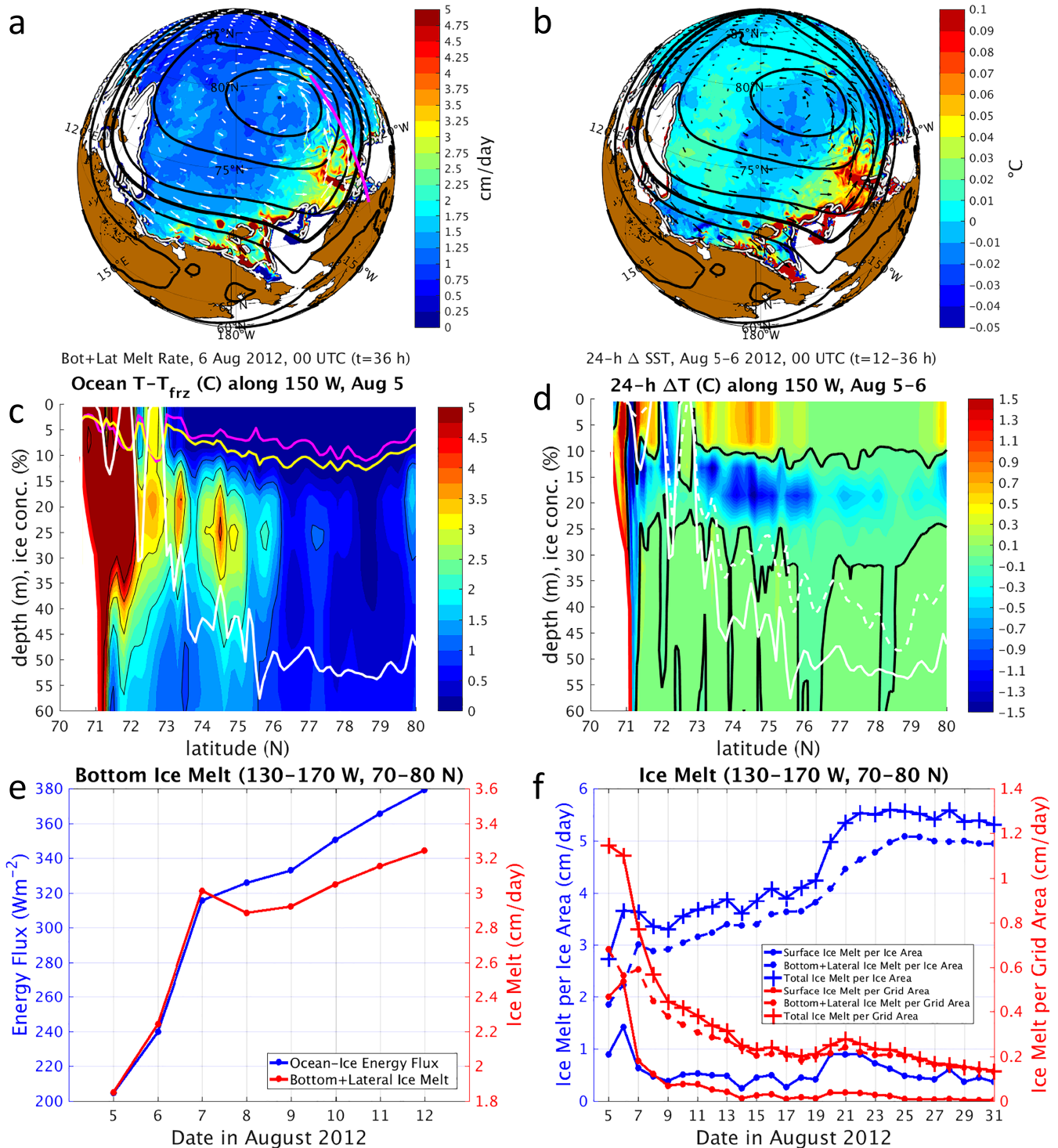


**Figure 2.** As in Figure 1 but for (a) the combined bottom and lateral melt rate, (b) the 24-hr change in SST, and vertical cross sections along 150°W (indicated by the magenta line in (a)) of (c) ocean temperature above freezing, and (d) the 24-hr change in ocean temperature. Note that (a) is instantaneous, whereas (b)–(d) are calculated from 24-hr mean fields. The 15% ice concentration contour is in solid white in (a) and (b). The solid white lines in (c) and (d) indicate the ice concentration along the cross section on 5 August, and the dashed white line in (d) indicates the concentration on 6 August, plotted on the same scale as the depth coordinate (e.g., 50% concentration is plotted at 50 m). The magenta and yellow lines in (c) indicate the thermodynamic mixed layer depth and the boundary layer depth defined by the Richardson number, respectively. The 0°C contour is in black in (d). (e) The ocean-ice heat flux and the instantaneous rate of bottom (plus lateral) melting, averaged over 130–170°W and 70–80°N (indicated by the magenta box in Figure 1a). (f) The surface, bottom (plus lateral), and total rate of melting, calculated per unit ice area (blue) and per unit grid cell area (red).

The region of non-negligible bottom melting (Figure 2a) is more widespread than that of surface melting, and there is more small-scale spatial variability. However, the bottom melting is clearly enhanced in the region beneath the maximum wind speed band (cf. Figures 2a and S1c), extending several degrees poleward of the ice edge. The heat flux from the ocean to ice (Figure 2e) is proportional to the difference between the SST and the freezing point of sea water (Hunke & Lipscomb, 2010), and so any process that increases the SST will tend to increase the rate of bottom melting. Figure 2b shows the 24-hr change in SST ( $\Delta$ SST) from 00 UTC 5 August to 00 UTC 6 August (excluding grid points with 100% open water). Though there are large tendencies near the ice edge,  $\Delta$ SST is very small over most of the ice-covered region of the Arctic, as the presence of concentrated ice strongly constrains the SST to be near the freezing point of sea water. Over portions of the Beaufort Sea beneath the cyclone, however, substantial warming of the oceanic mixed layer occurs, resulting in a region of enhanced bottom melting.

A vertical cross section of the ocean temperature above freezing along 150°W (Figure 2c) indicates that in the region of enhanced melting (73–76°N), there is a layer of much warmer water (2–4°C above freezing) from 15- to 35-m depth, just beneath the mixed layer (which is very near to the freezing temperature). This warm layer is a signature of the near-surface temperature maximum (NSTM), which is formed by absorption of shortwave radiation that penetrates through thin ice and leads (Jackson et al., 2010). As the ice melts and the mixed layer freshens, the heat of the NSTM is trapped beneath the mixed layer by the formation of a seasonal pycnocline (Steele et al., 2011) but can be mixed upward by turbulence induced by strong surface wind speeds. Evidence that the increase in SST on 6 August is a result of storm-induced turbulent mixing can be seen in Figure 2d, which shows the 24-hr change in temperature ( $\Delta$ T) along the same cross section as in Figure 2c. The region of warmer water beneath the mixed layer cools by up to 1.5°C, while the mixed layer itself warms by 0.25–1.0°C, which is indicative of turbulent entrainment. This is consistent with Zhang et al. (2013), who found in their PIOMAS simulation that parameterized vertical diffusivity within the upper ocean was greatly enhanced by the strong winds of (and ice motion induced by) the cyclone, mixing warmer water to the surface and increasing the rate of bottom melting.

Figure 2e shows the area-averaged (70–80°N and 130–170°W) heat flux from the ocean to the ice from 5 to 12 August, and it can be seen that there is a very good correspondence between the heat flux and the rate of bottom (plus lateral) melting, similar to that between the net surface energy budget and the surface melting shown in Figure 1f. The bottom melting is substantially greater than the surface melting, and whereas the surface melting beneath the cyclone peaks on 6 August, the bottom melting sharply increases from 5 to 7 August and then continues to increase more slowly after 8 August. The continued increase of bottom melting occurs because SST in this region keeps increasing throughout the month of August as the open water fraction increases (not shown). In part, this is because of the climatological tendency, but the cyclone itself has also accelerated the increasing SST through the mixing from the NSTM and the subsequent ice albedo feedback. Finally, Figure 2f compares (from 5–31 August) the surface and bottom melting when calculated per unit area of ice (as in Figures 1f and 2e) to the same terms when calculated per unit grid cell area. The former metric is appropriate for budget analyses and indicates how rapidly the ice itself is locally melting, whereas the latter metric is proportional to the integrated volume of ice loss. Although there is a clear signature of the cyclone on the local rate of melting, such a signature is difficult to discern in the integrated volume loss, because as the area covered by sea ice diminishes, there is simply less and less ice left to melt, regardless of the rate of melting of the ice that remains.

#### 4. Is there a Basin-Scale Impact on Sea Ice Loss?

Zhang et al. (2013) found that the total melting rate integrated over the entire Arctic (which is dominated by bottom melting) markedly increased in association with the cyclone, as can be seen in their Figure 2c, which we reproduce here as Figure 3a. Figure 3b shows an analogous time series of integrated melting rate for Navy-ESPC forecasts initialized at 12 UTC on 2, 3, and 4 August. In contrast to the PIOMAS simulation of Zhang et al. (2013), there is no clear signature of the cyclone on the area-integrated melting in the Navy-ESPC forecasts. The peak melting rate generally occurs at the beginning of each forecast in Navy-ESPC, and this melting rate is substantially greater than in PIOMAS for times that precede the cyclone. Figure 3c shows a time series of 24-hr ice volume change (integrated over the Arctic) for six different forecasts, and it is apparent that the signature of the cyclone that is evident in the PIOMAS analysis (distinct from the PIOMAS *forecast* shown in Figure 3a) is absent in the Navy-ESPC forecasts. It can also be seen that the first 4–8 days of each Navy-ESPC forecast exhibit anomalously large ice volume loss, regardless of initialization

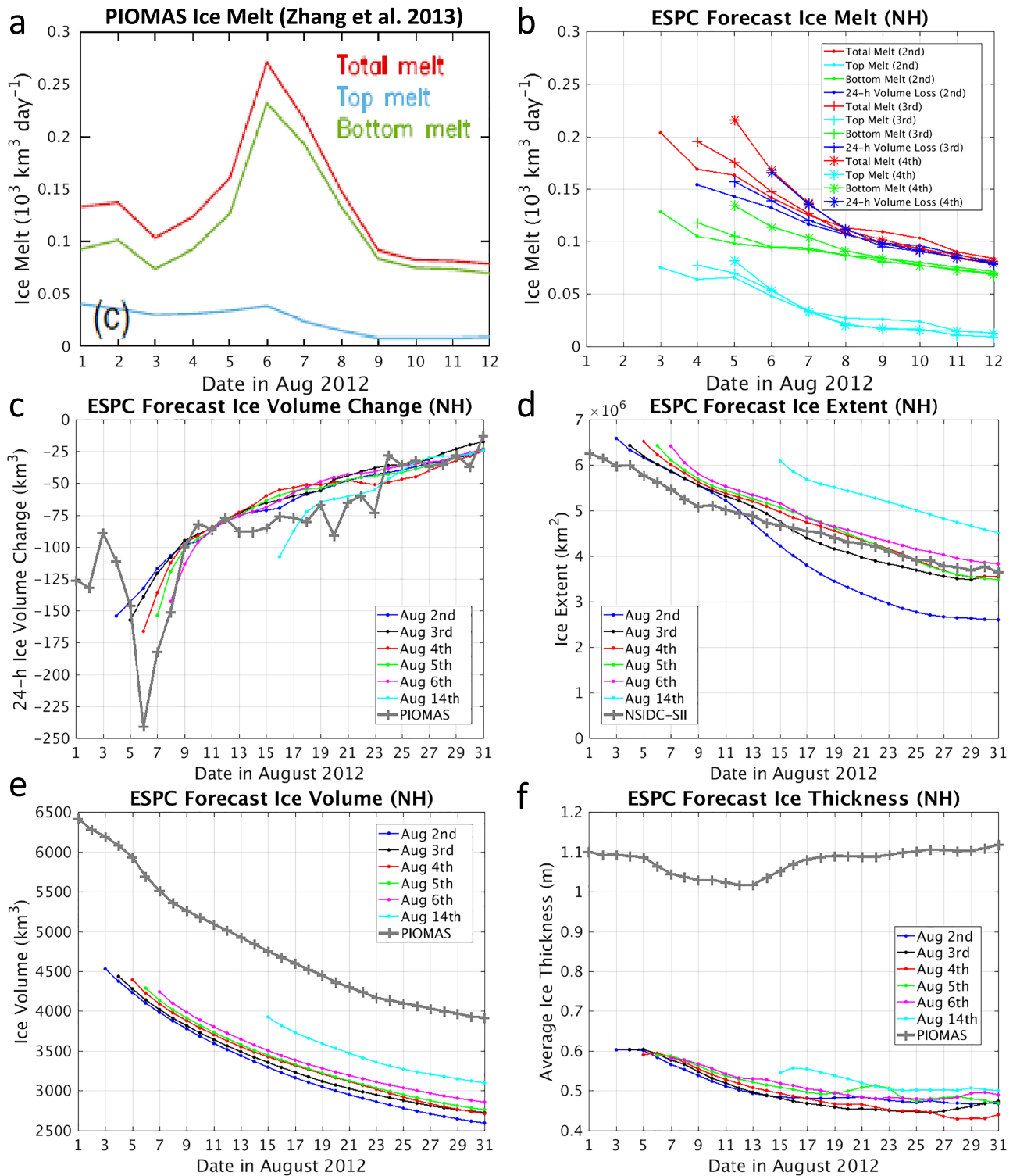


**Figure 3.** Time series of total (red), top (cyan), and bottom (green) melt for 1–12 August 2012 from (a) the PIOMAS simulation of Zhang et al. (2013, adapted from their Figure 2c) and (b) the Navy-ESPC forecasts initialized at 12 UTC on 2, 3, and 4 August. The blue lines in (b) show the 24-hr net loss of ice volume, which can be compared to the instantaneous total melt. For 1–31 August 2012, the Navy-ESPC forecast (c) ice volume change per 24 hr, (d) ice extent (defined by the area encompassed by grid boxes exceeding 15% ice concentration), (e) ice volume, and (f) mean ice thickness (averaged over grid boxes with thickness greater than 0.15 m). The Navy-ESPC fields in (c), (e), and (f) are compared to the PIOMAS analysis (distinct from the PIOMAS forecast in (a)), and the ice extent in (d) is compared to the NSIDC Sea Ice Index. Note that all fields in (a)–(f) are integrated or averaged over the Northern Hemisphere.

time (including 14 August, well after the cyclone) and then converge toward PIOMAS at longer lead times. This behavior may indicate that too much melting occurs near the beginning of Navy-ESPC forecasts, possibly due to an inconsistency between the initialization and the model physics. It is therefore also possible that the cyclone would otherwise have influenced the basin-scale sea ice loss in Navy-ESPC but that such a signature is masked by the biases early in the forecasts.

The Northern Hemispheric ice extent is shown in Figure 3d. Most of the Navy-ESPC forecasts initialized in early August compare relatively well in ice extent to the National Snow and Ice Data Center (NSIDC) Sea Ice Index. The initial extent is generally greater in Navy-ESPC than in the Sea Ice Index, which is likely related to the underestimation of ice concentration by passive microwave satellite sensors during the melt season (Meier et al., 2015). Navy-ESPC incorporates data from the 4-km Interactive Multisensor Snow and Ice Mapping System product from the National Ice Center, and this will tend to increase the ice extent over that estimated from microwave products alone (Hebert et al., 2015; Posey et al., 2015). Note that the initial extent decreases between successive forecasts substantially more slowly than the extent changes with time within each individual forecast, which again may indicate an inconsistency between the model physics and the initialization of ice. Specifically, we believe that the SST is too warm in areas where the data assimilation has introduced ice to initially ice-free grid cells. The assimilation of ice is uncoupled to the ocean variables in this version of Navy-ESPC, and in order to prevent overly rapid melting at such grid cells, the SST is incrementally cooled in the analysis in an ad hoc manner. It appears that the amount of imposed cooling is not great enough, resulting in ice that (nearly) immediately melts upon incorporation into the analysis.

We compare the integrated ice volume in the Navy-ESPC forecasts to the PIOMAS analysis in Figure 3e. Though the overall rate of ice volume loss is comparable, PIOMAS has 30–50% more ice volume than Navy-ESPC. The ice concentration is actually greater in Navy-ESPC than in PIOMAS over much of the marginal ice zone (not shown), and so the lesser ice volume in Navy-ESPC is associated with systematically thinner ice (Figure 3f). Though ice thickness is poorly constrained observationally, it is possible that the mean thickness and integrated volume are biased low in Navy-ESPC, as the PIOMAS reanalysis system has been tuned to agree relatively well with existing observations (Schweiger et al., 2011; 2019). On the other hand, PIOMAS has a known tendency for thickness to be biased *high* in regions of thin ice (Schweiger et al., 2011). We have compared Navy-ESPC analyses to PIOMAS and to the satellite-based CS2MOS estimate of ice thickness (Ricker et al., 2017) for corresponding times prior to the melt season of 2012 (satellite retrievals are unavailable during the melt season), and the satellite-retrieved sea ice thickness actually agrees better with Navy-ESPC than with PIOMAS over the Beaufort Sea (not shown). Ultimately, there remains substantial uncertainty in both models and satellite estimates regarding ice thickness, and more in situ observations are needed in order to better constrain the melt season distribution of sea ice thickness.

## 5. Discussion and Conclusions

Motivated by recent studies that have found that strong warm season cyclones may have a substantial influence on short-term rapid loss of sea ice, in this study we examined the effect of cyclone-induced melting in the fully coupled (atmosphere-ocean-ice) Navy-ESPC model. We found that concurrent with the passage of a cyclone over the Beaufort Sea in August of 2012, bottom melting was substantially enhanced in the marginal ice zone, as a consequence of turbulent entrainment of relatively warm water found at 15- to 35-m depth (the NSTM) into the oceanic mixed layer. This is consistent with the results of Zhang et al. (2013), who found in their PIOMAS simulation that vertical diffusivity greatly increased in response to the strong surface winds and resulting ice motion and that the warming of the mixed layer was the primary mechanism of cyclone-induced melting.

We also found that surface melting was enhanced in association with the cyclone, primarily due to anomalously strong sensible heating of the ice by the overlying atmosphere, which was maintained by the advection of warm air from over the open ocean and Alaska. This is in contrast to Zhang et al. (2013), who found that surface melting was much smaller in magnitude than bottom melting and that there was not a substantial increase in surface melting during the passage of the cyclone. It is difficult to directly compare our results for surface melting, both because Zhang et al. (2013) used daily-averaged forcing from the NCEP/NCAR reanalysis and because we only have instantaneous model output for the CICE component of Navy-ESPC at 00 UTC, which is afternoon over much of the Pacific sector of the Arctic. Even where there is 24-hr daylight, the diurnal cycle of shortwave radiation is large, and so the rate of surface melting seen in Figure 1 for

Navy-ESPC is larger than for a corresponding 24-hr mean. The representation of clouds and radiation in both models and reanalyses for the Arctic is also notoriously poor (Barton et al., 2012; Inoue et al., 2006; Lindsay et al., 2014; Tjernström et al., 2008; Walsh et al., 2009), and direct observations of the surface energy budget are rare (Persson et al., 2002), and so it is possible that Navy-ESPC simulates too much incoming shortwave radiation, which could result in a high bias in surface melting. Nevertheless, we have determined that the primary source of the local enhancement of surface melting in the Navy-ESPC forecast is the anomalous sensible heating, not the shortwave radiation, and so our result that surface melting is substantially enhanced in association with the cyclone should not be that sensitive to the lack of a diurnal cycle in our analyses or to potential biases in cloud cover in Navy-ESPC. The 2-m air temperature distribution within the warm sector of the cyclone in Navy-ESPC is similar to that of both ERA-Interim and the ASR2 reanalysis (not shown) (Bromwich et al., 2018). In contrast, the temperature is several degrees cooler in the NCEP/NCAR reanalysis that is used to force PIOMAS (not shown). Therefore, it is possible that the effect of the cyclone on locally enhancing surface melt is underestimated in PIOMAS.

Although the effect of the strong cyclone of August 2012 on the melting of sea ice in Navy-ESPC is locally large, this influence is spatially confined and relatively transient. The enhanced surface melting only occurs where surface air temperatures are able to substantially exceed 0°C, and this is necessarily limited to the region near to the ice edge, as flow over the ice mitigates the warm air advection, and the eventual occlusion of the baroclinic cyclone cuts off the source of warm air. The enhanced bottom melting is also limited to the region near the ice edge, because a prominent NSTM only exists where the ice is thin and sparse enough to have allowed for substantial absorption of shortwave radiation that penetrated through the ice and the oceanic mixed layer. As is seen in Figure 2c, the warm layer is not pronounced poleward of 76°N, where the ice concentration exceeds 50%. Because of these limiting factors, it appears difficult for an individual cyclone to greatly reduce the sea ice volume over the Arctic Ocean as a whole, and indeed, we found in Navy-ESPC that neither the ice volume integrated over the Arctic nor the ice extent was noticeably altered in association with the cyclone. This differs from Zhang et al. (2013), who did see a clear signature of the cyclone on basin-wide melting and sea ice extent in PIOMAS. Note, however, that Meier et al. (2015) showed that the microwave-retrieved sea ice concentration product used for validation by Zhang et al. (2013) (and which is assimilated into PIOMAS analyses) greatly overestimated the decrease of sea ice extent in association with the cyclone. Finally, sea ice extent can also be changed by the redistribution of ice from advection and convergence (unlike integrated volume which is only affected by melting). Although we did not examine these dynamic influences on sea ice extent in the Navy-ESPC forecasts, the time series of extent and volume changes are highly correlated, and so the thermodynamic influence on sea ice extent must be dominant, and this is consistent with the conclusions of Zhang et al. (2013).

Because of the large uncertainties in both observations and models, it is difficult to determine whether the true response of the sea ice to the cyclone of August 2012 is closer to the results of our study or to those of Zhang et al. (2013). We plan to further investigate the source of the discrepancies between the respective simulations in a future study, where we will force the ice and ocean components of Navy-ESPC with the same NCEP/NCAR reanalysis atmosphere used by Zhang et al. (2013), which will help to separate the effects of differences in forcing from differences in model physics. We note that there remains a critical need for in situ observations that can be used to identify systematic model biases, which is necessary in order for improving both short-term and seasonal forecasts within the Arctic.

The storm of August 2012 was unusually strong and by some metrics was the strongest melt season Arctic cyclone on record (Simmonds & Rudeva, 2012). The response to this cyclone therefore potentially represents an upper bound for cyclone-induced melting of sea ice, and even for this extreme case, the contribution to Arctic-wide loss of sea ice appears to be relatively limited. Even though Zhang et al. (2013) find a substantial short-term effect of this cyclone on sea ice extent (in contrast to our results), they determined that the ultimate seasonal minimum extent was only changed by a few percent in response to the cyclone. As Arctic cyclones are typically not nearly as strong as the 2012 case, it stands to reason that Arctic-wide sea ice extent and sea ice volume are unlikely to be greatly affected by individual cyclones, on average. Indeed, several recent studies have found that increased melting and reduced sea ice extent tend to be associated instead with *anticyclonic* anomalies (Ding et al., 2017; Wernli & Papritz, 2018). Although there are conflicting results regarding the long-term trend of cyclone activity in the Arctic, there does not appear to be any clear tendency toward stronger or more frequent extreme cyclones (Koyama et al., 2017). On the other hand, as sea ice extent continues its long-term decline, it is possible that the mechanisms by which individual cyclones

locally enhance melting become more widespread, as heat storage in the NSTM layer becomes larger over a broader area. Future studies are necessary to further refine our understanding of the role of cyclones on the melting of sea ice.

### Acknowledgments

This research was supported by the Office of Naval Research Arctic Cyclone DRI (Program Element 0601153N). We thank UW/PWS for the PIOMAS data, which is available online (<http://psc.apl.uw.edu/research/projects/arctic-sea-ice-volume-anomaly/data/>). Simulations used in this study are archived online (<http://iridl.ldeo.columbia.edu/SOURCES/.Models/.SubX/.NRL/>).

### References

- Barton, N., Janiga, M., McLay, J., Reynolds, C., Rowley, C., Hogan, P., & Thoppil, P. (2019). Earth system prediction capability (ESPC) initial operational capability (IOC) ensemble system (*Tech. Rep. NRL/MR/7532-19-9928*). Washington, D.C.: Naval Research Laboratory.
- Barton, N. P., Klein, S. A., Boyle, J. S., & Zhang, Y. Y. (2012). Arctic synoptic regimes: Comparing domain-wide Arctic cloud observations with CAM4 and CAM5 during similar dynamics. *Journal of Geophysical Research Atmospheres*, *117*, D15205. <https://doi.org/10.1029/2012JD017589>
- Bromwich, D. H., Wilson, A. B., Bai, L., Liu, Z., Barlage, M., Shih, C.-F., et al. (2018). The Arctic System Reanalysis, version 2. *Bulletin of the American Meteorological Society*, *99*, 805–828.
- Ding, Q., Schwiager, A., L'Heureux, M., Battisti, D. S., Po-Chedley, S., Johnson, N. C., et al. (2017). Influence of high-latitude atmospheric circulation changes on summertime Arctic sea ice. *Nature Climate Change*, *7*, 289–296.
- Flocco, D., Schroeder, D., Feltham, D. L., & Hunke, E. C. (2012). Impact of melt ponds on Arctic sea ice simulations from 1990 to 2007. *Journal of Geophysical Research*, *117*, C09032. <https://doi.org/10.1029/2012JC008195>
- Hebert, D. A., Allard, R. A., Metzger, E. J., Posey, P. G., Preller, R. H., Wallcraft, A. J., et al. (2015). Short-term sea ice forecasting: An assessment of ice concentration and ice drift forecasts using the U.S Navy's Arctic Cap Nowcast/Forecast System. *Journal of Geophysical Research: Oceans*, *120*, 8327–8345. <https://doi.org/10.1002/2015JC011283>
- Hogan, T. F., Liu, M., Ridout, J. A., Peng, M. S., Whitcomb, T. R., Ruston, B. C., et al. (2014). The Navy Global Environmental Model. *Oceanography*, *27*, 116–125.
- Hunke, E. C., & Lipscomb, W. H. (2010). CICE: The Los Alamos Sea Ice Model documentation and software user's manual version 4.1 (*Tech. Rep. LA-CC-06-012*). Los Alamos N.M.: Los Alamos Natl Lab.
- Inoue, J., Liu, J., Pinto, J. O., & Curry, J. A. (2006). Intercomparison of Arctic regional climate models: Modeling clouds and radiation for SHEBA in May 1998. *Journal of Climate*, *19*, 4167–4178.
- Jackson, J. M., Carmack, E. C., McLaughlin, F. A., Allen, S. E., & Ingram, R. G. (2010). Identification, characterization, and change of the near-surface temperature maximum in the Canada Basin, 1993–2008. *Journal of Geophysical Research*, *115*, C05021. <https://doi.org/10.1029/2009JC005265>
- Jackson, J. M., Williams, W. J., & Carmack, E. C. (2012). Winter sea-ice melt in the Canada Basin, Arctic Ocean. *Geophysical Research Letters*, *39*, L03603. <https://doi.org/10.1029/2011GL050219>
- Kay, J. E., L'Ecuyer, T., Gettelman, A., Stephens, G., & O'Dell, C. (2008). The contribution of cloud and radiation anomalies to the 2007 Arctic sea ice extent minimum. *Geophysical Research Letters*, *35*, L08503. <https://doi.org/10.1029/2008GL033451>
- Koyama, T., Stroeve, J., Cassano, J., & Crawford, A. (2017). Sea ice loss and Arctic cyclone activity from 1979 to 2014. *Journal of Climate*, *30*, 4735–4754.
- Lindsay, R., Wensnahan, M., Schweiger, A., & Zhang, J. (2014). Evaluation of seven different atmospheric reanalysis products in the Arctic. *Journal of Climate*, *27*, 2588–2606.
- Lüpkes, C., Vihma, T., Jakobson, E., König-Langlo, G., & Tetzlaff, A. (2010). Meteorological observations from ship cruises during summer to the central Arctic: A comparison with reanalysis data. *Geophysical Research Letters*, *37*, L09810. <https://doi.org/10.1029/2010GL042724>
- Meier, W. N., Fetterer, F., Stewart, J. S., & Helfrich, S. (2015). How do sea-ice concentrations from operational data compare with passive microwave estimates? Implications for improved model evaluations and forecasting. *Annals of Glaciology*, *56*, 332–340.
- Meier, W. N., & Stewart, J. S. (2019). Assessing uncertainties in sea ice extent climate indicators. *Environmental Research Letters*, *14*, 035005.
- Metzger, E. J., Smedstad, O. M., Thoppil, P. G., Hurlburt, H. E., Cummings, J. A., Wallcraft, A. J., et al. (2014). US Navy operational global ocean and Arctic ice prediction systems. *Oceanography*, *27*, 32–43.
- Park, H.-S., Lee, S., Son, S.-W., Feldstein, S. B., & Kosaka, Y. (2015). The impact of poleward moisture and sensible heat flux on Arctic winter sea ice variability. *Journal of Climate*, *28*, 5030–5040.
- Parkinson, C. L., & Comiso, J. C. (2013). On the 2012 record low Arctic sea ice cover: Combined impact of preconditioning and an August storm. *Geophysical Research Letters*, *40*, 1356–1361. <https://doi.org/10.1002/grl.50349>
- Pegion, K., Kirtman, B. P., Becker, E., Collins, D. C., LaJoie, E., Burgman, R., et al. (2019). The subseasonal experiment (SubX): A multi-model subseasonal prediction experiment. *Bulletin of the American Meteorological Society*, *100*, 2043–2060.
- Perovich, D. K., Richter-Menge, J. A., Jones, K. F., & Light, B. (2008). Sunlight, water, and ice: Extreme Arctic sea ice melt during the summer of 2007. *Geophysical Research Letters*, *35*, L11501. <https://doi.org/10.1029/2008GL034007>
- Persson, P. O. G., Fairall, C. W., Andreas, E. L., Guest, P. S., & Perovich, D. K. (2002). Measurements near the atmospheric surface flux group tower at SHEBA: Near-surface conditions and surface energy budget. *Journal of Geophysical Research*, *107*(C10), 8045.
- Posey, P. G., Metzger, E. J., Wallcraft, A. J., Hebert, D. A., Allard, R. A., Smedstad, O. M., et al. (2015). Improving Arctic sea ice edge forecasts by assimilating high horizontal resolution sea ice concentration data into the US Navy's ice forecast systems. *The Cryosphere*, *9*, 1735–1745.
- Ricker, R., Hendricks, S., Kaleschke, L., Tian-Kunze, X., King, J., & Haas, C. (2017). A weekly Arctic sea-ice thickness data record from merged CryoSat-2 and SMOS satellite data. *The Cryosphere*, *11*, 1607–1623.
- Schweiger, A., Lindsay, R., Zhang, J., Steele, M., Stern, H., & Kwok, R. (2011). Uncertainty in modeled Arctic sea ice volume. *Journal of Geophysical Research*, *116*, C00D06. <https://doi.org/10.1029/2011JC007084>
- Schweiger, A., Wood, K., & Zhang, J. (2019). Arctic sea ice volume variability over 1901–2010: A model-based reconstruction. *Journal of Climate*, *32*, 4731–4752.
- Serreze, M. C., Stroeve, J., Barret, A. P., & Boisvert, L. N. (2016). Summer atmospheric circulation anomalies over the Arctic Ocean and their influences on September sea ice extent: A cautionary tale. *Journal of Geophysical Research: Atmospheres*, *121*, 11,463–11,485. <https://doi.org/10.1002/2016JD025161>
- Simmonds, I., & Rudeva, I. (2012). The great Arctic cyclone of August 2012. *Geophysical Research Letters*, *39*, L23709. <https://doi.org/10.1029/2012GL054259>
- Steele, M., Ermold, W., & Zhang, J. (2011). Modeling the formation and fate of the near-surface temperature maximum in the Canadian Basin of the Arctic Ocean. *Journal of Geophysical Research*, *116*, C11015. <https://doi.org/10.1029/2010JC006803>
- Steele, M., Zhang, J., & Ermold, W. (2010). Mechanisms of summertime upper Arctic Ocean warming and the effect on sea ice melt. *Journal of Geophysical Research*, *115*, C11004. <https://doi.org/10.1029/2009JC005849>

- Stroeve, J., Hamilton, L. C., Bitz, C. M., & Blanchard-Wrigglesworth, E. (2014). Predicting September sea ice: Ensemble skill of the SEARCH Sea Ice Outlook 2008–2013. *Geophysical Research Letters*, *41*, 2411–2418. <https://doi.org/10.1002/2014GL059388>
- Tjernström, M., Sedlar, J., & Shupe, M. (2008). How well do regional climate models reproduce radiation and clouds in the Arctic? An evaluation of ARCMIP simulations. *Journal of Applied Meteorology and Climatology*, *47*, 2405–2422.
- Walsh, J. E., Chapman, W. L., & Portis, D. H. (2009). Arctic cloud fraction and radiative fluxes in atmospheric reanalyses. *Journal of Climate*, *22*, 2316–2334.
- Watanabe, E., & Ogi, M. (2013). How does the summer wind modulate sea ice-ocean heat balance in the Canada Basin? *Geophysical Research Letters*, *40*, 1569–1574. <https://doi.org/10.1002/grl.50363>
- Wernli, H., & Papritz, L. (2018). Role of polar anticyclones and mid-latitude cyclones for Arctic summertime sea-ice melting. *Nature Geoscience*, *11*, 108–113.
- Woods, C., & Caballero, R. (2016). The role of moist intrusions in winter Arctic warming and sea ice decline. *Journal of Climate*, *29*, 4473–4485.
- Yamagami, A., Matsueda, M., & Tanaka, H. L. (2018). Predictability of the 2012 Great Arctic Cyclone on medium-range timescales. *Political Science*, *15*, 13–23.
- Zhang, J., Lindsay, R., Schweiger, A., & Steele, M. (2013). The impact of an intense summer cyclone on 2012 Arctic sea ice retreat. *Geophysical Research Letters*, *40*, 720–726. <https://doi.org/10.1002/grl.50190>
- Zhang, J., & Rothrock, D. A. (2003). Modeling global sea ice with a thickness and enthalpy distribution model in generalized curvilinear coordinates. *Monthly Weather Review*, *131*, 681–697.